JJMIE

Volume 1, Number 1, Sep. 2007
ISSN 1995-6665
Pages 57 - 67

Jordan Journal of Mechanical and Industrial Engineering

A Graphical Design of an Input-Shaping Controller for Quay-Side Container Cranes with Large Hoisting: Theory and Experiments

Ziyad N. Masoud [a,*], Mohammed F. Daqaq [b]

[a] Department of Mechanical Engineering, The Hashemite University, Zarqa 13115, Jordan
[b] Department of Mechanical Engineering, Clemson University, Clemson, SC 29634, USA

Abstract

Input-shaping is a practical open-loop strategy for the control of transient and residual oscillations on cranes, especially those having predefined payload transfer paths and repeated maneuvers. In this paper double-step input-shaping control approach is developed to include maneuvers that involve large hoisting distances and speeds. The approach is based on using the graphical representation of the phase plane of the payload oscillations. The phase plane is used to derive mathematical constraints to compute the switching times of a double-step acceleration command profile that will result in minimal transient and residual oscillations. The controller design is based on a two-dimensional four-bar-mechanism model of a container crane. For the purpose of controller design, the model is reduced to a constrained double pendulum with variable length hoisting cable and a kinematic angular constraint. The generated commands were based on both a linear and a nonlinear frequency approximations of the payload oscillation period. Numerical and experimental results demonstrated that in contrast with the single-step input shaping controllers, which are very sensitive to frequency approximations, the proposed double-step controller is less sensitive to small variations in the frequency even with large commanded accelerations. Using this approach, oscillations during and at the end of transfer maneuvers can be reduced to less than 5 cm on a full size model of a 65 ton quay-side container crane.

Keywords: Input-shaping; container crane; crane control.

1. Introduction

Motion control of suspended objects has seen mounting research interest since the early 1960's. The dynamics of such systems are used to model the dynamics of the payload oscillations in many important industrial applications, such as gantry cranes, boom cranes, ship-mounted cranes, telescopic cranes, and quay-side container cranes.

A particularly important case is that of a quay-side container crane, Fig. 1. Inertial forces on the payload due to crane commanded trajectories can cause the payload to experience large sway oscillations. To avoid exciting these oscillations, crane operators resolve to slowing down the operations such that the oscillations do not cause safety concerns and possible damage of the payload. However, slowing down operations increases the cost of loading and unloading operations.

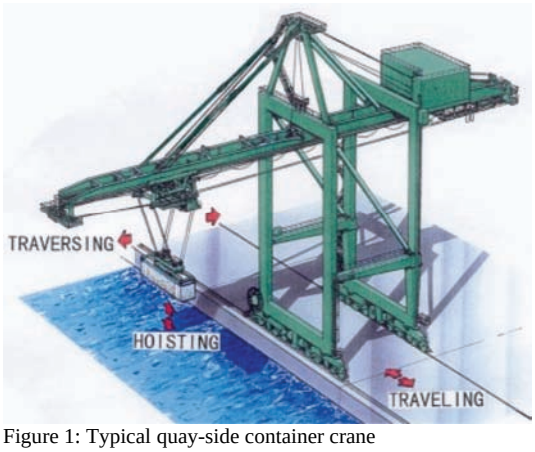

Figure 1: Typical quay-side container crane

In contrast with other types of cranes, which are usually modeled as a simple pendulum with a rigid or flexible hoisting cable and a lumped mass at its end [1–7], quay-side container cranes have a significantly different configuration. The actual hoisting mechanism of a

* Corresponding author. e-mail: zmasoud@hu.edu.jo

container crane consists typically of a set of four hoisting cables arrangement. The cables are hoisted from four different points on a trolley and are attached on the payload side to four points on a spreader bar used to lift containers.

Cargo transfer control varies according to the crane application. For example, in one application large oscillations maybe acceptable during the transfer operation, however, the settling time, overshoot, and the magnitude of residual oscillations are kept minimal at the end of the transfer maneuver to allow for accurate cargo positioning. In other applications, such as nuclear reactors, or where the space around the crane is populated, the safety requirements are very strict. Thus large oscillations are not acceptable during and at the end of a transfer maneuver.

Input-shaping control is an old but still widely used strategy to control suspended objects in general, and container cranes in particular. Its effectiveness comes from the fact that it does not require alterations to the original structure of the crane, or the installation of additional mechanical hardware. However, these controllers are not generally robust. Their performance is very sensitive to changes in system parameters, time delays, external disturbances, and they require "highly accurate values of the system parameters" to achieve satisfactory system response [8–10]. While a good design can minimize the controller's sensitivity to changes in the payload mass, it is much harder to alleviate the controller's sensitivity to changes in the hoisting cable length.

Alsop et al. [11] were the first to propose a controller based on input-shaping. The controller was used to automate an ore unloader, by accelerating the trolley in steps of constant acceleration then killing the acceleration when the payload reaches zero oscillation angle (after multiples of a full oscillation period). The trolley then coasts at constant speed along the path for a period of time necessary to complete the transfer maneuver. A replicate of the acceleration procedure is used in the deceleration stage. The switching times for the acceleration and deceleration steps were calculated using an iterative computer procedure. They also used a linear frequency approximation of a simple pendulum model. Their results demonstrated very little residual oscillations, while transient oscillation angles were of order of 10° during the acceleration/deceleration stages.

Nonlinear frequency approximation of a simple pendulum was also used to improve the performance of the single-step controllers [12, 13]. Numerical simulations demonstrated that an acceleration profile based on the nonlinear frequency approximation can dampen the residual oscillations two orders of magnitude more than that based on a linear frequency approximation. The enhanced performance was most pronounced for longer coasting distances and higher accelerations.

Alzinger and Brozovic [14] showed that a double-step acceleration profile results in significant reductions in travel time over a single-step acceleration profile. Testing on an actual crane has shown that the double-step acceleration profile can deliver both faster travel and minimal payload oscillations at the target point.

Starr [15] used a symmetric double-step acceleration shaped profile to transport a suspended object with minimal oscillations. A linear approximation of the period of the payload is used to calculate the switching times and to generate an analytical expression for the acceleration profile. This work was later extended by employing a nonlinear approximation of the payload frequency to generate single-step and double-step symmetric acceleration profiles [16].

Using a new approach, Jansen, and Noakes [17] showed analytically that input-shaping is equivalent to a notch filter applied to a general input signal and centered around the natural frequency of the payload. They applied a second-order robust notch filter to shape the acceleration input. Numerical simulation and experimental verification of this strategy on an actual bidirectional gantry crane, moving under arbitrary step accelerations and changing cable length at a very slow constant rate, showed that the strategy was able to suppress residual payload oscillation. The work was extended by developing a command shaping notch filter to reduce payload oscillation on rotary cranes excited by the operator commands. It was reported that in general, there was no guarantee that applying such filter to the operator's commands would result in excitation terms having the desired frequency content, and that it only works for low speed and acceleration commands [18]. Results were later verified experimentally [19].

Singhose et al. [20] developed four different input-shaping controllers. They reported that the best controller produced a reduction of 73% in transient oscillations over the time-optimal rigid-body commands. However, they noticed that "transient deflection with shaping increases with hoist distance, but not as severely as the residual oscillations". The numerical simulations showed that "the percentage in reduction with shaping is dependent on system parameters". As a result, the four controllers suffered significant degradation in performance when applied to crane maneuvers that involved hoisting.

Daqaq et al. [21] developed a single-step input-shaping controller for quay-side container cranes. The controller was based on a four-bar-mechanism model of the crane [22, 23]. The model was simplified to a double-pendulum model with kinematic constraints. The method of multiple scales was used to find an analytical nonlinear expression for the period of oscillation in both the acceleration and coasting modes. They reported that a single-step input shaping controller based on a simple pendulum fails when applied to quay-side container cranes. In fact their results showed that such controller may amplify the residual oscillations to large magnitudes. On the other hand, numerical simulations showed that a controller based on the nonlinear frequency approximation of the double-pendulum model of the crane results in a superior performance. To increase the controller performance robustness, they combined the shaped commands with a nonlinear delayed-position feedback at the end of the transfer operation.

In this paper, a graphical phase plane approach is used to derive geometric constraints that are used to develop a double-step input-shaping controller that accounts for large hoisting operations. The graphically derived constraints are combined with physical constraints, then solved numerically for the switching times of the acceleration profile. The controller is based on a four-bar-mechanism model of the container crane. Switching times were

calculated using both linear and nonlinear frequency approximations of this model. Experiments were conducted on a 1:10 scaled model of a 65 ton quay-side container crane with a 7 m track and 3.5 m hoisting cables.

2. Mathematical Modeling

In this section, a four-bar-mechanism is developed to model the actual hoisting mechanism of the quay-side container crane capturing all dynamic and geometrical constraints of the mechanism. This model is later transformed to a double-pendulum model with kinematic constraints equivalent to those of the four-bar-mechanism model. However, numerical simulations are performed on the full model of the crane.

2.1. Full Model

Figure.2 shows a two-dimensional side projection of a quay-side container crane. This four-bar-mechanism is developed to model the actual dynamics of the hoisting mechanism of the crane. The container is grabbed using a spreader bar, which is then hoisted from the trolley by means of four cables, two of which are shown. The cables are spaced a distance *d* at the trolley and a distance *w* at the spreader bar. The hoisting cables in the model are treated as rigid massless inextensible links with variable lengths. The specific equations of these scleronomic holonomic constraints are

$$\Phi(\mathbf{q},t)=\begin{bmatrix}\left(x+R\sin\theta-\frac{1}{2}w\cos\theta-f+\frac{1}{2}d\right)^2\\ \quad+\left(y-R\cos\theta-\frac{1}{2}w\sin\theta\right)^2-L^2\\ \left(x+R\sin\theta-\frac{1}{2}w\cos\theta-f-\frac{1}{2}d\right)^2\\ \quad+\left(y-R\cos\theta+\frac{1}{2}w\sin\theta\right)^2-L^2\end{bmatrix}=0 \quad (1)$$

where $\mathbf{q}=[x,y,\theta]^T$ is the generalized coordinates vector.

Using the Lagrange multipliers, one can write the set of differential-algebraic equations DAE's [24] as

$$\begin{bmatrix}\mathbf{M} & \Phi_{\mathbf{q}}^T\\ \Phi_{\mathbf{q}} & 0\end{bmatrix}\begin{bmatrix}\ddot{\mathbf{q}}\\ \Lambda\end{bmatrix}=\begin{bmatrix}\mathbf{Q}^A\\ \Gamma\end{bmatrix} \quad (2)$$

where $\mathbf{M}=diag[m,m,m\bar{k}^2]$ is the inertia matrix, m is the mass of the load and the spreader bar, $\bar{k}$ is the combined radius of gyration of the load and spreader bar about point Q, $\mathbf{Q}^A=[0,-mg,0]^T$ is the generalized applied force vector, Λ are the Lagrange multipliers, and

$$\Gamma=-(\Phi_{\mathbf{q}}\dot{\mathbf{q}})_{\mathbf{q}}-2\Phi_{\mathbf{qt}}\dot{\mathbf{q}}-\Phi_{tt} \quad (3)$$

where the subscripts denote partial derivatives.

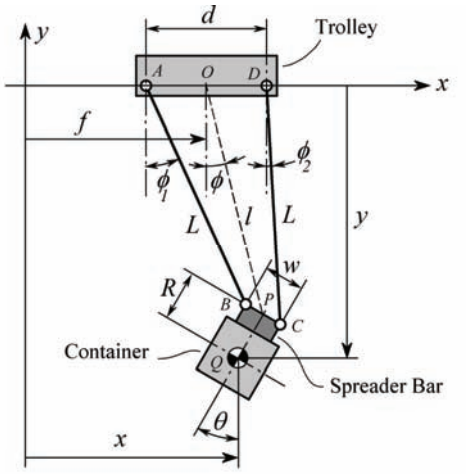

Figure 2: A schematic model of a container crane

2.2. Double-Pendulum Model

To better understand the dynamics of the system, and to derive analytical expression for the system frequency which is essential to the controller design, the four-bar-mechanism model is transformed into a double-pendulum system with a variable length cable *l*, a rigid body with a mass center at a distance *R* from the midjoint of the double pendulum, and a kinematic constraint relating the angles ϕ and θ as shown in Fig. 3.

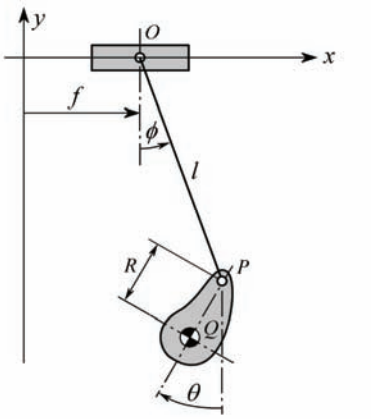

Figure 3: A schematic of a constrained double pendulum model of a container crane

Point *O* In Fig. 2 is the midpoint between points *A* and *D*, and point *P* is the midpoint between points *B* and *C*. The closing equations of the loop *ABPO* are

$$l\sin\phi-\frac{1}{2}w\cos\theta+\frac{1}{2}d=L\sin\phi_1 \quad (4)$$

$$l\cos\phi-\frac{1}{2}w\sin\theta=L\cos\phi_1 \quad (5)$$

Similarly, the closing equations of the loop *ODCP* can be written as

$$l\sin\phi+\frac{1}{2}w\cos\theta-\frac{1}{2}d=L\sin\phi_2 \quad (6)$$

$$l\cos\phi+\frac{1}{2}w\sin\theta=L\cos\phi_2 \tag{7}$$

Squaring and adding Eqs. (4) and (5), and squaring and adding Eqs. (6) and (7), we can eliminate L, ϕ_1, and ϕ_2 from the resulting equations and obtain the following relations

$$\theta=-\phi+\sin^{-1}\left(\frac{d}{w}\sin\phi\right) \tag{8}$$

$$l=\sqrt{L^2-\frac{1}{4}(d^2+w^2-2dw\cos\theta)} \tag{9}$$

Equation (8) represents the kinematic constraint between the angles ϕ and θ. Applying Eqs. (8) and (9) to the double-pendulum model results in a kinematic behavior identical to the four-bar-mechanism model. The position vector to the center of mass of the payload of the constrained double pendulum is

$$\mathbf{r}=(f+l\sin\phi-R\sin\theta)\mathbf{i}-(l\cos\phi+R\cos\theta)\mathbf{j} \tag{10}$$

Using Eq. (10), we write the kinetic and potential energies of the constrained double pendulum as

$$\begin{aligned}T=&\frac{1}{2}ml^2\dot{\phi}^2+\frac{1}{2}m(\bar{k}^2+R^2)\dot{\theta}^2+\frac{1}{2}m\dot{f}^2\\&-mRl\dot{\phi}\dot{\theta}\cos(\phi+\theta)+ml\dot{\phi}\dot{f}\cos\phi-mR\dot{\theta}\dot{f}\cos\theta\end{aligned} \tag{11}$$

$$V=-mg(l\cos\phi+R\cos\theta) \tag{12}$$

Substituting the constraint Eqs. (8) and (9) into Eqs. (11) and (12) results in the elimination of θ from the energy expressions of the system. To derive the equation of motion that describes the time variation of ϕ, the Euler-Lagrange equations are used which are given as

$$\frac{d}{dt}\left(\frac{\partial\mathcal{L}}{\partial\dot{\phi}}\right)-\frac{\partial\mathcal{L}}{\partial\phi}=0 \tag{13}$$

where $\mathcal{L}=T-V$. Substituting Eqs. (11) and (12) in Eq. (13) results in the full nonlinear equation of motion for the double pendulum model. Due to the lengthy expressions in this equation, only the linear first order expansion is shown as

$$\ddot{\phi}+2\mu\dot{\phi}+\omega_o^2\phi+\frac{\mu}{2\dot{L}}\ddot{f}=0 \tag{14}$$

where

$$\begin{aligned}\omega_o^2&=\frac{g(L+a^2R)-a\dfrac{dR\ddot{L}}{w}}{L^2-2aRL+a^2(\bar{k}^2+R^2)}\\\mu&=\frac{\dot{L}(L-aR)}{L^2-2aRL+a^2(\bar{k}^2+R^2)}\\a&=\frac{d-w}{w}\end{aligned} \tag{15}$$

In the above linear approximation, we assume that $l\approx L$. For small angles of oscillation ϕ, this assumption results in a maximum error of 1% in calculating the length l based on typical values of d, w, and L for container cranes.

3. Controller Design

Analyzing the dynamics involved in Eq. (14) forms a basis for designing the double-step input-shaping controller. To find the equilibrium solution, ϕ_L, we let $\dot{\phi}=\ddot{\phi}=0$ in Eq. (14) to get

$$\phi_L=-\frac{L-aR}{g(L+a^2R)-a\dfrac{dR\ddot{L}}{w}}\ddot{f} \tag{16}$$

For constant cable length operations, $\dot{L}=\ddot{L}=0$, the linearized system has a single stationary fixed-point given by

$$\phi_o=-\frac{L-aR}{g(L+a^2R)}\ddot{f} \tag{17}$$

This equilibrium solution is a marginally stable center. For constant L, the solution of Eq. (14) is illustrated in the phase portraits shown in Fig. 4(a). The figure shows that the solution is periodic with the payload exhibiting a limit cycle behavior. The center of the resulting limit cycle along the ϕ axis is determined by the amplitude and sign of the equilibrium solution ϕ_o. The radius of the resulting limit cycle is determined by the payload initial angular displacement and velocity.

For operations that involve hoisting, the dynamic behavior of the payload is qualitatively different. The variation of L causes the equilibrium solution described by Eq. (16) to vary along the ϕ axis. This kind of equilibrium solution is known as a non-stationary equilibrium point. Moreover, in the case of hoisting ($\dot{L}\neq0$) the term including $\dot{\phi}$ in Eq. (14) is no longer equal to zero. This term will act as a damping term with the sign of $\dot{L}$ determining the type of damping. The equilibrium solution of Eq. (14) is no longer a marginally stable center. The stability of this equilibrium solution is now determined by the sign of $\dot{L}$. For a positive $\dot{L}$, the damping is positive and the equilibrium solution is a stable focus (sink). On the other hand, for a negative $\dot{L}$, the damping is negative and the equilibrium solution is an unstable focus (source). The qualitative dynamic behavior of the payload around the non-stationary equilibrium solution is illustrated in Fig. 4(b) and Fig. 4(c).

Figure 5 shows a typical acceleration profile for a double-step input-shaping controller. The trolley accelerates at a constant rate of a_{max} for time t_{a1}, after which the trolley coasts at a constant velocity until time t_{c1}. The trolley then accelerates again with the same acceleration amplitude a_{max} until time t_{a2} at which the acceleration phase is concluded. Afterwards, the trolley coasts until time T, then decelerates in two steps similar to the acceleration stage. The switching times of the acceleration phase are calculated so that the trolley reaches the design velocity with zero payload oscillations. Similarly, the switching times of the deceleration phase are calculated so that the payload oscillations caused by the trolley deceleration are eliminated at the trolley stop.

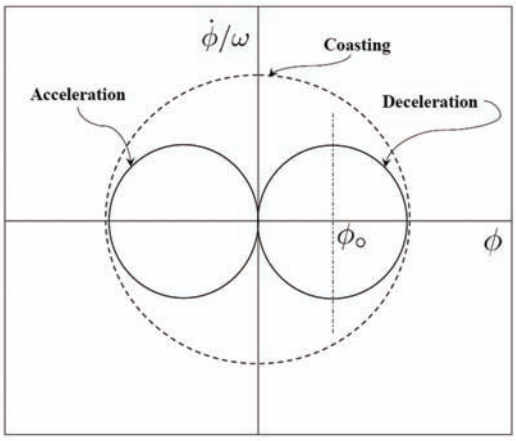

(a) $\dot{L} = 0$.

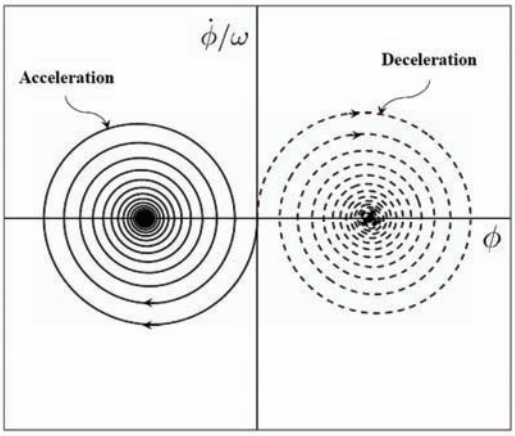

(b) $\dot{L} > 0$.

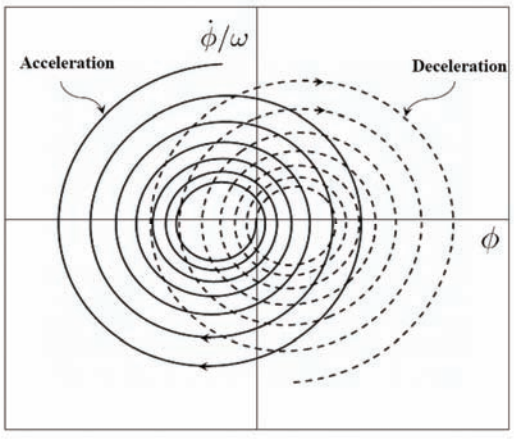

(c) $\dot{L} < 0$.

Figure 4: Phase portraits describing the dynamics of the crane payload

The shaped double-step acceleration profile like the one shown in Fig. 5 uses the maximum system capabilities (acceleration and speed) to achieve the required transfer maneuver with minimal transient and residual oscillations. To generate the required profile, the switching times are calculated such that the payload dynamics follow the phase portrait shown in Fig. 6. Ideally, this phase portrait drives the dynamics of the payload to end at the equilibrium point at the center of the phase portrait rather than a limit cycle around it.

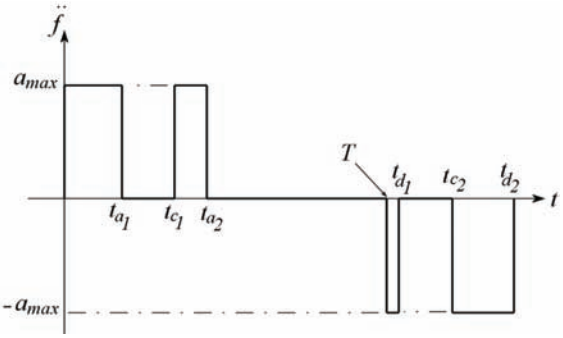

Figure 5: Typical acceleration profile of a double-step input-shaping controller

To determine the switching times for the required phase portrait, the trolley acceleration profile must satisfy two sets of constraints. The first set includes the dynamic constraints that involve the amplitudes of the response at the beginning and at the end of each acceleration step, and the physical constraints on the crane motors. The second set includes geometrical constraints derived from the phase portrait of the shaped acceleration and deceleration profiles.

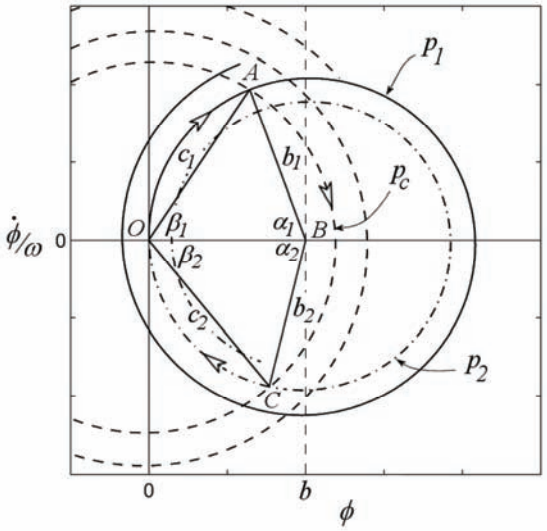

Figure 6: Graphical representation of the controller phase portrait.

Since L is slowly varying when compared to ϕ, the damping term associated with $\dot{\phi}$ can be treated as constant when analyzing the fast dynamics of the system for short periods of time. This assumption does not imply slow cable hoisting. The variation of L is only slow when compared to the fast variation of the angle ϕ. Hence, to derive these dynamic constraints, we assume that the system response is exponentially damped. Furthermore, for typical crane parameters and operating range of the hoisting cable, the equilibrium solution is assumed stationary. An average damping is used over each acceleration and coasting step as

$$\mu_{ave} = \frac{1}{t_2 - t_1} \int_{t_1}^{t_2} \mu(\tau)\, d\tau \qquad (18)$$

In the first acceleration step, the trolley accelerates so that the new equilibrium solution is at point *B*, Fig. 6. The response follows the path p_1 through a phase angle α_1 to point *A*. The amplitude of the response at that point is

$$b_1 = b\,\mathrm{e}^{\mu_{ave} t_{a1}} \tag{19}$$

The second acceleration step t_{c1} to t_{a2} is designed to force the response of the system to home at the origin of the phase portrait at the end of this acceleration step. The system response follows the path p_2 through the phase angle α_2. Going back in time, the starting amplitude of oscillation of the second acceleration step at point *C* has to satisfy

$$b_2 = b\,\mathrm{e}^{-\mu_{ave}(t_{a2} - t_{c1})} \tag{20}$$

To guarantee the continuity of the response, points *A* and *C* are required to fall on the same coasting path p_c in the phase portrait. This can be represented by the following relation

$$c_2 = c_1\,\mathrm{e}^{-\mu_{ave}(t_{c_1} - t_{a_1})} \tag{21}$$

Equations (19), (20), and (21) represent the first three equations of the dynamics set of constraints. The fourth dynamic constraint is derived from the physical limitations on the velocity and acceleration achievable by the trolley motors. This constraint can be enforced by restricting the acceleration time so that the trolley velocity does not exceed the maximum achievable velocity by the trolley motors.

$$v_{max} = a_{max}(t_{a_1} + t_{a_2} - t_{c_1}) \tag{22}$$

The second set of constraints is derived directly from the graphical representation of the controller phase portrait, Fig. 6. Graphically, the coasting phase is split into two consecutive stages: β_1 and β_2. The first phase ends when the response crosses the zero velocity axis on the phase portrait at time t_o. Considering the upper triangle *OAB*, and using the geometric laws of sines and cosines, the following geometric constraints are obtained

$$c_1^2 = b^2 + b_1^2 - 2bb_1\cos\alpha_1 \tag{23}$$

$$c_1 = b_1\frac{\sin\alpha_1}{\sin\beta_1} \tag{24}$$

Similarly, considering the lower triangle *OCB*, two geometric constraints are also derived as

$$c_2^2 = b^2 + b_2^2 - 2bb_2\cos\alpha_2 \tag{25}$$

$$c_2 = b_2\frac{\sin\alpha_2}{\sin\beta_2} \tag{26}$$

The phase angles of the controlled performance in the acceleration and coasting phases can be related to the system frequencies and switching times by the following equations

$$\alpha_1 = \int_0^{t_{a1}} \omega_a\,dt \tag{27}$$

$$\alpha_2 = \int_{t_{c1}}^{t_{a2}} \omega_a\,dt \tag{28}$$

$$\beta_1 = \int_{t_{a1}}^{t_o} \omega_c\,dt \tag{29}$$

$$\beta_2 = \int_{t_o}^{t_{c1}} \omega_a\,dt \tag{30}$$

where ω_a and ω_c are the frequency of payload oscillations in the accelerations and coasting stages, respectively. When a linear frequency approximation is used, $\omega_a = \omega_c = \omega_o$.

The constraint equations Eqs. (19) – (26) can be reduced to four equations in terms of the unknown switching times t_{a1}, t_o, t_{c1}, and t_{a2} by substituting Eqs. (19), (24), (27), and (29) into Eq. (23)

$$\mathrm{e}^{2\mu_{ave}t_{a1}}\frac{\sin^2\left(\int_0^{t_{a1}}\omega_a\,dt\right)}{\sin^2\left(\int_{t_{a1}}^{t_o}\omega_c\,dt\right)} = 1 + \mathrm{e}^{2\mu_{ave}t_{a1}} - 2\,\mathrm{e}^{\mu_{ave}t_{a1}}\cos\left(\int_0^{t_{a1}}\omega_a\,dt\right) \tag{31}$$

Similarly, Eqs. (20), (26), (28), and (30) are substituted into Eq. (25) to get

$$\mathrm{e}^{-2\mu_{ave}(t_{a2}-t_{c1})}\frac{\sin^2\left(\int_{t_{c1}}^{t_{a2}}\omega_a\,dt\right)}{\sin^2\left(\int_{t_o}^{t_{c1}}\omega_c\,dt\right)} = 1 + \mathrm{e}^{-2\mu_{ave}(t_{a2}-t_{c1})} - 2\,\mathrm{e}^{-\mu_{ave}(t_{a2}-t_{c1})}\cos\left(\int_{t_{c1}}^{t_{a2}}\omega_a\,dt\right) \tag{32}$$

Equations (19), (20), (24), (26), and (27) – (30) are also substituted into Eq. (21)

$$\mathrm{e}^{-\mu_{ave}t_{a2}}\frac{\sin\left(\int_{t_{c1}}^{t_{a2}}\omega_a\,dt\right)}{\sin\left(\int_{t_o}^{t_{c1}}\omega_c\,dt\right)} = \frac{\sin\left(\int_{t_o}^{t_{a1}}\omega_a\,dt\right)}{\sin\left(\int_{t_{a1}}^{t_o}\omega_c\,dt\right)} \tag{33}$$

The final set of four constraint equations Eqs. (22), and Eqs. (31) – (33) are then numerically solved for the switching times of the controller. This approach is used for both the acceleration and deceleration stages. The trolley coasting time between the acceleration and deceleration stages is determined by the total travel distance of the trolley.

4. Numerical Simulations

To simplify the calculations, the following simulations are designed so that the trolley acceleration stages fall within the constant hoisting speed stage. This is done to avoid discontinuities in the hoisting profile which results from the square hoist acceleration profile. This approach speeds up the calculation time to the point where it becomes feasible to implement this approach on standard PLC controllers used on quay-side container cranes. The maximum hoisting acceleration used in these simulations is 0.75 m/s^2 and the maximum hoisting velocity is 1.5 m/s. In the numerical simulations the following crane dimensions are used: d = 2.82 m, w = 1.41 m, R = 2.5 m, and $\bar{k}$ = 1.0 m. The payload mass is m = 50,000 kg.

Using the linear frequency approximation Eq. (15) a shaped double-step acceleration profile is generated for a fixed cable-length transfer operation. The resulting profile is applied to the full model equations of motion Eqs. (2). The numerically simulated response is shown in Fig. 7.

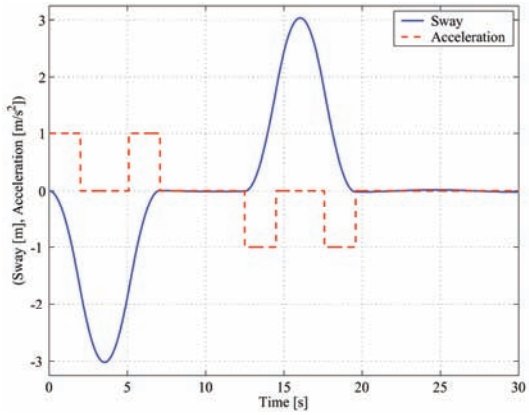

(a) Payload sway and trolley acceleration

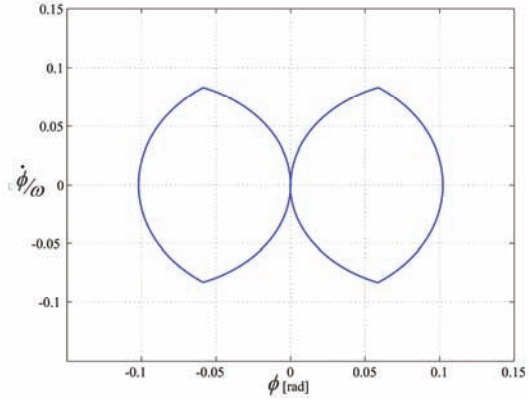

(b) Phase portrait of the response

Figure 7: Sway response of a container crane to shaped operator commands. Results are obtained for L = 32.5 m, S = 50 m

Daqaq et. al. [21] reported that for single-step input shaping control strategy, a controller based on a nonlinear frequency approximation of the payload oscillations results in a superior performance when compared to that based on a linear approximation. To check the effect of using a nonlinear frequency approximation on the performance of the double-step input-shaping controller, we will use the linear frequency approximation and the nonlinear frequency approximation developed earlier [21]. The nonlinear approximation is dependent on the oscillation amplitude and the trolley acceleration, hence $\omega_a \neq \omega_c \neq \omega_o$.

Figure. 8 illustrates a comparison between the performance of the double-step input-shaping controller using the linear and nonlinear frequency approximations. The amplitude of the residual oscillation resulting from a linear frequency approximation is larger than that resulting from a nonlinear approximation. However, in contrast with the single-step input-shaping controller where the difference is as large as 10 orders of magnitude, the difference here is very small and can be tolerated. This is due to the fact that using the double-step profile the period over which large oscillations occur is so short that the effects of the difference between the linear and nonlinear frequency approximations does not yield significant deviation from the desired system dynamics.

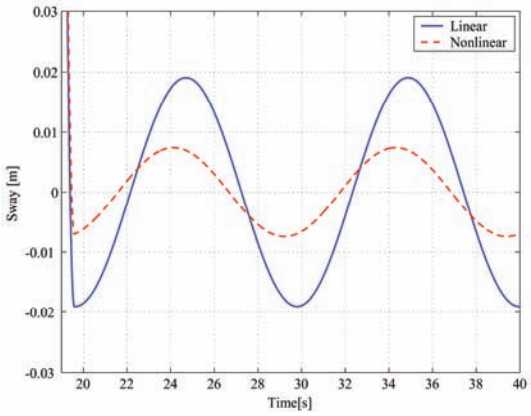

Figure 8: Residual oscillations of the payload resulting from a double-step input-shaping controller, L = 32:5 m, and S = 50 m

Several transfer maneuvers are simulated, three of which are presented here to demonstrate a hoisting up, lowering, and a combined hoisting up and lowering maneuvers. In the first simulation, the payload is transferred a distance of 50 m. During the transfer operation the payload is hoisted up 15 m starting from a position 35 m below the trolley with an acceleration of 0.75 m/s^2, after the hoist acceleration is concluded in the first two seconds, the trolley starts to accelerate with a maximum acceleration of 0.5 m/s^2 to reach a maximum velocity of 3 m/s, Fig. 9(a). The payload motion trajectory is shown in Fig. 9(b), and the controller switching times are listed in Table 1. The total payload transfer operation is conducted in 25.6 seconds. The maximum oscillation magnitude after the acceleration stage is 12.2 mm, and 15.4 mm at the end of the transfer maneuver. Figures 9(c) and 9(d) show the phase portrait of the system and the payload oscillation throughout the transfer maneuver.

Table 1: Switching times for a hoisting maneuver from L_i to L_f.

L_i (m)	L_f (m)	t_{a1} (sec)	t_o (sec)	t_{c1} (sec)	t_{a2} (sec)
35	20	2.5762	3.6751	3.9538	7.3777
20	20	3.0000	3.1859	3.3717	6.3717
20	25	3.3145	3.4186	3.9776	6.6632
20	35	3.4601	3.6677	4.7279	7.2678

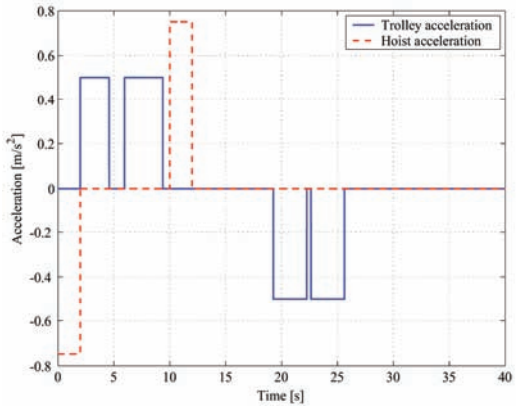

(a) Trolley and hoist accelerations

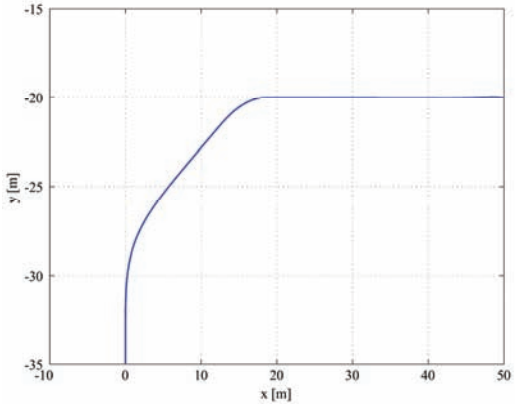

(b) Motion profile

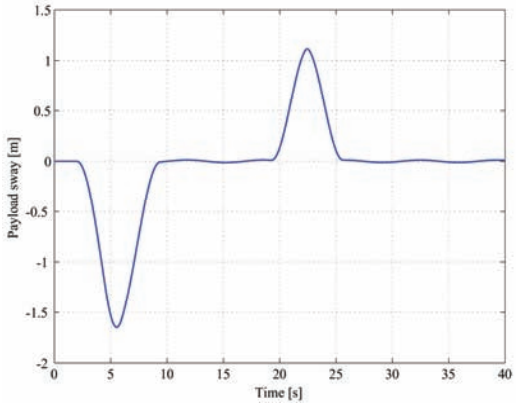

(c) Payload sway

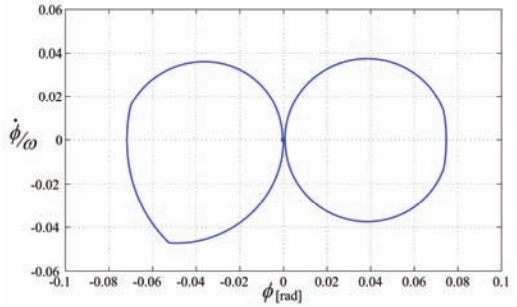

(d) Phase portrait

Figure 9: A transfer operation involving a 15 m hoisting

In the second simulation, the payload is transferred 50 m starting from a position 20 m below the trolley. During the transfer operation the payload is lowered 15 m with an acceleration of 0.75 m/s^2, Fig. 10(a). The payload motion trajectory is shown in Fig. 10(b). The system performance is shown in Fig. 10(c) and Fig. 10(d). The total transfer operation is concluded in 26.3 seconds. The magnitude of the resulting payload oscillations after the acceleration stage is 12.5 mm and 11.4 mm at the end of the transfer maneuver.

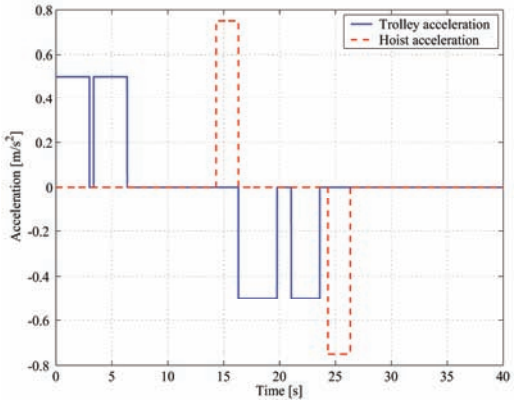

(a) Trolley and hoist accelerations

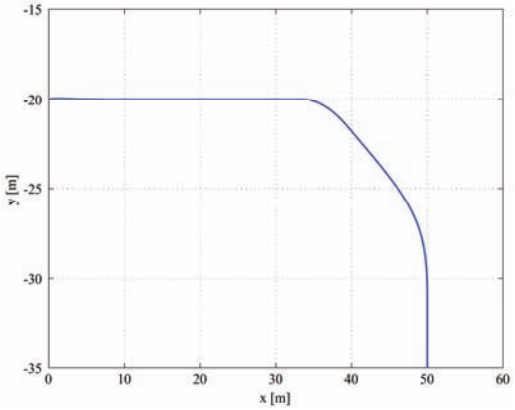

(b) Motion profile

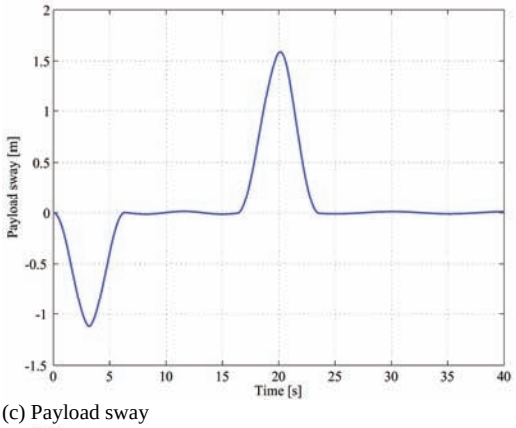

(c) Payload sway

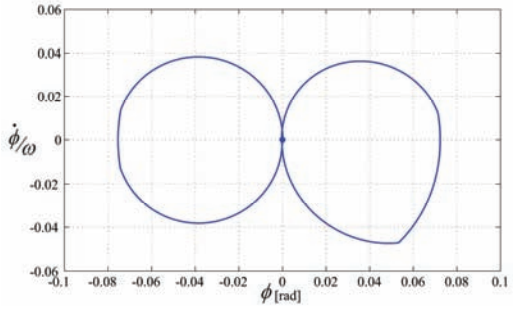

(d) Phase portrait

Figure 10: A transfer operation involving a 15 m lowering

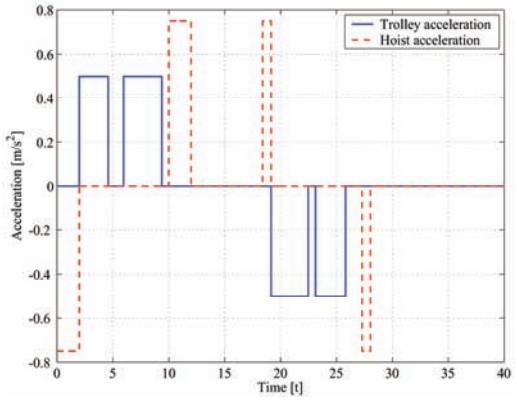

(a) Trolley and hoist accelerations

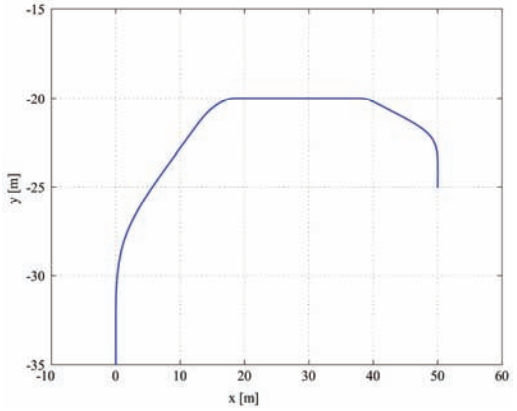

(b) Motion profile

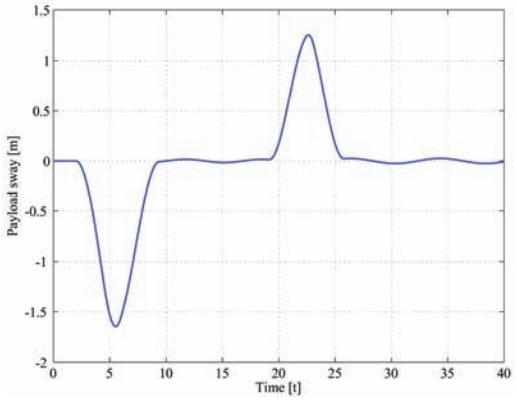

(c) Payload sway

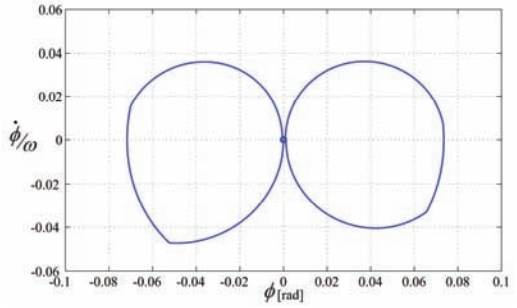

(d) Phase portrait

Figure 11: A transfer operation involving a 15 m hoisting and a 5 m lowering

In the third simulation, the payload is transferred 50 m starting from a position 35 m below the trolley. During the transfer operation the payload is hoisted up 15 m then lowered 5 m, Fig. 11(b). The system performance is shown in Fig. 11(c) and. 11(d). The total transfer operation is concluded in 28 seconds. The magnitude of the resulting payload oscillations after the acceleration stage is 15.4 mm and 25 mm at the end of the transfer maneuver.

5. Experimental Testing

To validate the controller design approach and the numerical simulations, a 1:10 scale model of a 65 ton quay-side container crane was constructed, as shown in Fig. 12. The support mechanism consists of two 7 m tracks and a trolley driven by a DC brushless servomotor. The motor has a 4000 *rpm* rated speed, 510 N.m continuous torque, and 1.5 *hp* rated power. The hoist mechanism consists of four steel cables connected to four aluminum pulleys on the trolley and to four points on the spreader bar. The spreader bar is attached to a 1:10 scale model of a standard 20 ft container. The four pulleys are driven using two DC brushless servomotors.

Several tests were conducted. Two tests are presented here. Two performance factors are used as measures for the controller performance. The first is that the controller incorporates the maximum crane speeds and accelerations, which guarantees the conclusion of the transfer maneuver in minimal time. The second is that the magnitude of the residual oscillations is less than 5 mm (equivalent to 50 mm on the full scale crane) at the end of the transfer maneuver.

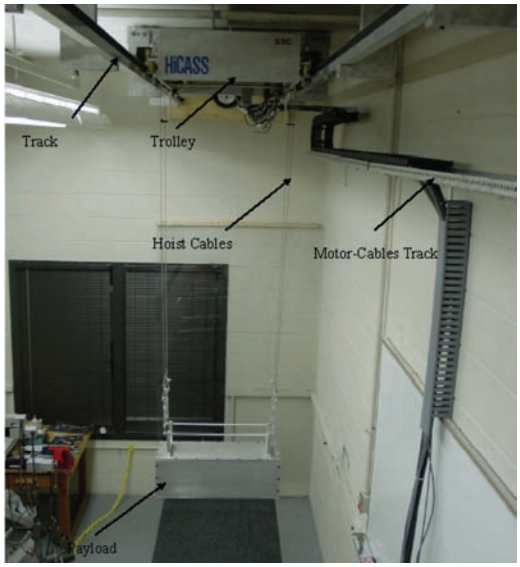

Figure 12: A 1:10 scale model of a 65-ton quay-side container crane

In the first test, the trolley travels a distance of 5 m. During the transfer maneuver, the payload is lowered 1.5 m starting from a position 2 m below the trolley with an acceleration of 0.5 m/s^2. The payload motion trajectory is shown in Fig. 13(a). The trolley starts to accelerate with a maximum acceleration of 0.5 m/s^2 to reach a maximum velocity of 1 m/s, Fig. 13(b). The total transfer maneuver is concluded in 8.4 seconds. At the end of the acceleration phase of the maneuver, the maximum magnitude of oscillations was less than 4 mm. When the transfer

maneuver was concluded, the maximum magnitude of the residual oscillations was less than 4.5 mm. Figure 13(c) illustrates the payload sway throughout the transfer maneuver.

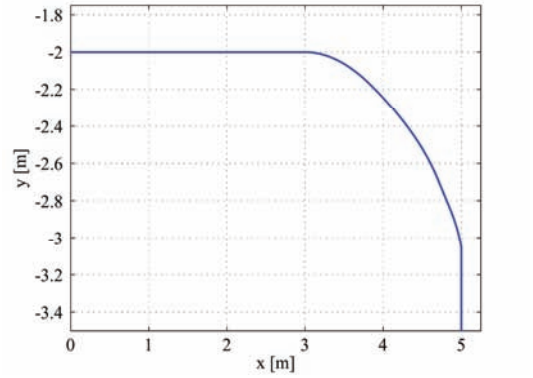

(a) Motion profile

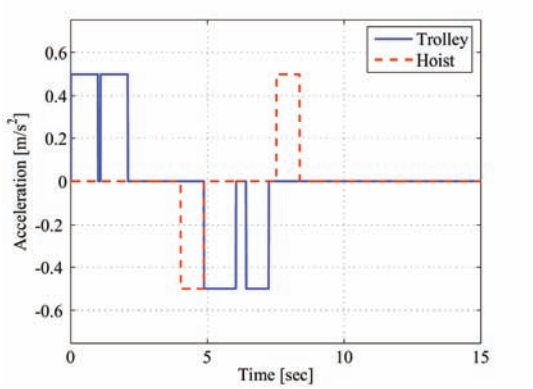

(b) Trolley and hoist accelerations

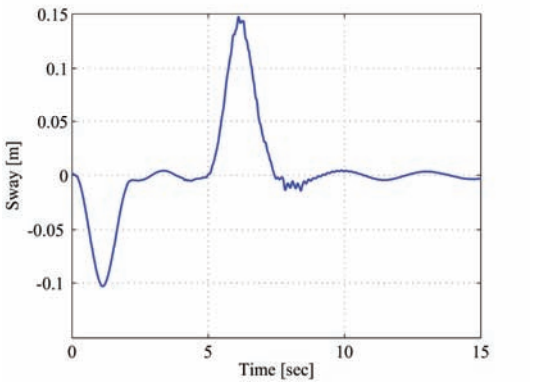

(c) Payload sway

Figure 13: A 5 m payload transfer operation involving a 1.5 m lowering

In the second test, the payload is moved a distance of 5 m. During the transfer maneuver, the payload is first hoisted up 1.5 m starting from a position 3.5 m below the trolley, travels for a short time, and is then lowered 1.5 m. The payload motion trajectory is shown in Fig. 14(a). The trolley starts to accelerate with a maximum acceleration of 0.5 m/s^2 to reach a maximum velocity of 1 m/s and the payload is hoisted and lowered with a maximum acceleration of 0.5 m/s^2 to reach a maximum speed of 1 m/s, Fig. 14(b). The total transfer maneuver is concluded in 9.2 seconds. The maximum magnitude of oscillations was less than 4.2 mm at the end of the acceleration stage and less than 4.5 mm at the end of the transfer maneuver. Figure 14(c) illustrates the payload sway throughout the transfer maneuver.

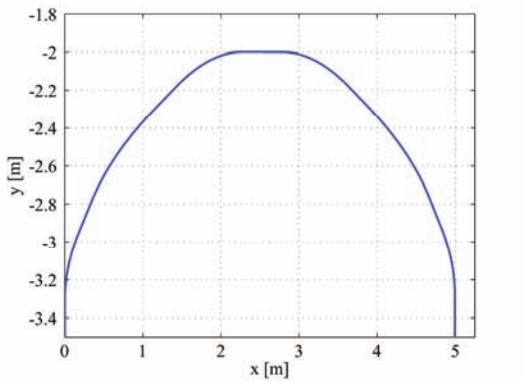

(a) Motion profile

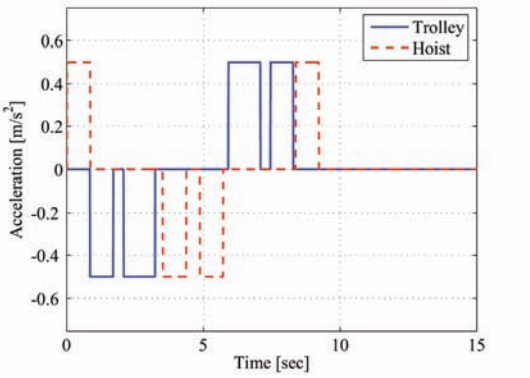

(b) Trolley and hoist accelerations

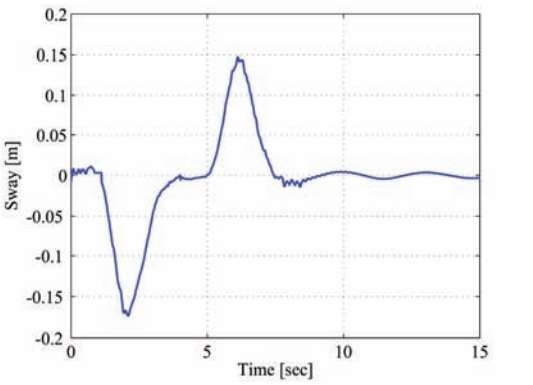

(c) Payload sway

Figure 14: A 5 m payload transfer operation involving a 1.5 m hoisting then 1.5 m lowering

Many other tests were conducted involving different hoisting and lowering maneuvers. In all cases, the residual oscillations were less than 5 mm in magnitude.

6. Conclusions Remarks

A double-step input-shaping controller is developed for sway oscillation control of quay-side container crane operations that involve large hoisting maneuvers. This approach is based on the graphical representation of the phase portrait that describes the response of the payload of a container crane to a double-step acceleration profile.

During operations involving large hoist speeds and distances, the quasi-static approach to system modeling fails, especially for open-loop control systems, which require accurate and proper system identification. The hoisting speed has a significant effect on the system frequency and the dynamic response of the payload. Hoisting can either excite or dampen oscillations depending on the direction of the hoisting action.

Double-step input-shaping controllers are less sensitive to the nonlinearity of the frequency approximation. The short acceleration times made possible by the ability of the controller to utilize the maximum crane acceleration and speed makes using a linear approximation of the frequency sufficient for switching times calculations. However, simple pendulum frequency approximation is far from the actual frequency of quay-side container cranes. In fact, the frequency approximation must be based on a model that includes the multi-cable hoisting mechanism of the crane. The approximation used in this work was derived using a four-bar-mechanism model of the hoisting system of the crane and carried sufficient accuracy for input-shaping control design purposes.

The performance predicted by the numerical simulations of this work was validated experimentally on a 1:10 scaled model of a 65 ton quay-side container crane. Negligible differences in the amplitudes of the residual oscillations in the simulations and experiments were observed due to unmodeled friction and the fact that the hoisting cables are wrapped around pulleys rather than attached to “points” on the trolley.

Both numerical and experimental tests satisfied the shipping industry standard of less that 50 mm of sway for accurate container positioning.

References

[1] Abdel-Rahman, E. M., Nayfeh, A. H., and Masoud, Z. N., Dynamics and Control of Cranes: A Review, Journal of Vibrations and Control, 44, 2003, 863-908.

[2] d'Andrea-Novel, B., Boustany, F., and Conrad, F., Control of an Overhead Crane: Stabilization of Flexibilities, in Boundary Control and Boundary Variation: Proceedings of the IFIP WG 7.2 Conference, Sofia Antipolis, France, 1990, 1-26.

[3] d'Andrea-Novel, B., Boustany, F., Conrad, F., and Rao, B. P., Feedback stabilization of a hybrid PDE-ODE system: Application to an overhead crane, Mathematics of Controls, Signals, and Systems, 7, 1994, 1-22.

[4] d'Andrea-Novel, B., Boustany, F., Control of an Overhead Crane: Feedback Stabilization of a Hybrid PDE-ODE System: in Proceedings of the 1st European Control Conference: ECC 91, Grenoble, France, 1991, 2244-2249.

[5] Joshi, S. and Rahn, C. D., Position Control of a Flexible Cable of a Gantry Crane: Theory and Experiment, in Proceedings of the American Control Conference, Seattle, WA, 1995, 301-305.

[6] Martindale, S. C., Dawson, D. M., Zhu, J., and Rahn, C. D., Approximate Nonlinear Control for a Two Degree of Freedom Overhead Crane: Theory and Experimentation, in *Proceedings of the American Control Conference*, Seattle, WA, 1995, 301-305.

[7] Rahn, C. D., Zhang, F., Joshi, S., and Dawson, D. M., Asymptotically Stabilizing Angle Feedback for a Flexible Cable Gantry Crane, *Journal of Dynamic Systems, Measurement, and Control, 15*, 1999, 563-566.

[8] Zinober, A. S. I., The Self-Adaptive Control of an Overhead Crane Operations, in *Proc. of the 5th IFAC Symposium on Identification and System Parameter Estimation*, Darmstadt, East Germany, 1979, 1161-1167.

[9] Virkkunen, J. and Marttinen, A., Computer control of a loading bridge, in *Proceedings of the IEE International Conference: Control '88*, Oxford, UK, 1988, 484-488.

[10] Yoon, J. S., Park, B. S., Lee, J. S., and Park, H. S., Various control schemes for implementation of the anti-swing crane, in *Proceedings of the ANS 6th Topical Meeting on Robotics and Remote Systems*, Monterey, CA, 1995, 472-479.

[11] Alsop, C. F., Forster, G. A., and Holmes, F. R., Ore Unloader Automation - A Feasibility study, in *Proc. of IFAC Workshop on Systems Engineering for Control Systems*, Tokyo, Japan, 1965, 295-305.

[12] Jones, J. F. and Petterson, B. J., Oscillation damped movement of suspended objects, in *Proc. of the IEEE International Conference on Robotics and Automation*, Philadelphia, PA, 1988, 956-962.

[13] Dadone, P. , and Vanlandinham, H. F., Load Transfer Control for a Gantry Crane with Arbitrary Delay Constraints, *Journal of Vibration and Control, 7*, 2001, 135-158.

[14] Alzinger, E., and Brozovic, V., Automation and Control System for Grab Cranes, *Brown Boveri Review,Vol. 7*, 1983, 351-356.

[15] Starr, G. P., Swing-free transport of suspended objects with a path-controlled robot manipulator, *Journal of Dynamic Systems, Measurement, and Control, 107*, 1985, 97-100.

[16] Strip, D. R., Swing-free transport of suspended objects: A general treatment, *IEEE Transactions on Robotics and Automation, 5(2)*, 1989, 234{236.

[17] Kress, R. L., Jansen, J. F., and Noakes, M. W., Experimental implementation of a robust damped-oscillation control algorithm on a full-sized, two-degree-of-freedom, AC induction motor-driven crane, in *Proceedings of the 5th International Symposium on Robotics and Manufacturing: Research, Education, and Applications: ISRAM'94*, Maui, HI, 1994, 585-592.

[18] Parker, G. G., Groom, K., Hurtado, J., Robinett, R. D., and Leban, F., Command shaping boom crane control system with nonlinear inputs, in *Proceedings of the IEEE International Conference on Control Applications, 2*, Kohala Coast, HI, 1999, 1774-1778.

[19] Parker, G. G., Groom, K., Hurtado, J. E., Feddema, J., Robinett, R. D., and Leban, F., Experimental verification of a command shaping boom crane control system, in *Proceedings of the American Control Conference, 1*,San Diego, CA, 1999, 86-90.

[20] Singhose, W. E., Porter, L. J., and Seering, W. P., Input shaped control of a planar crane with hoisting, in *Proceedings of the American Control Conference*, Albuquerque, NM, 1997, 97-100.

[21] Daqaq, M. F., Masoud Z. N., and Nayfeh, A. H., Nonlinear Modeling and Control of Quay-Side Container Cranes, in *Proceedings of The IMAC-XXIII Conference and Exposition on Structural Dynamics*, Orlando, Fl, 2005.

[22] Masoud, Z., and Nayfeh, A. H., Sway Reduction on Container Cranes Using Delayed Feedback Controller, in *Proceedings of the AIAA*, Denver, CO, 2002.

[23] Masoud, Z., and Nayfeh, A. H., Sway Reduction on Container Cranes Using Delayed Feedback Controller, *Nonlinear Dynamics, 34 (3-4)*, 2003, 347-358.

[24] Blajer, W., and Kolodziejczyk, A., A geometric approach to solving problems of control constraints: theory and a DAE framework, in *Multibody Syst. Dyn.Vol.11,No.4*, 2004, 343-364.